



Keyhole-in-keyhole formation by adding a coaxially superimposed single-mode laser beam in disk laser deep penetration welding

M. Möbus¹ · P. Woizeschke²

Received: 1 August 2022 / Accepted: 20 January 2023 / Published online: 10 February 2023
© The Author(s) 2023

Abstract

Laser deep penetration welding is characterized by the formation of a vapor capillary (keyhole) and a high overall absorption (coupling rate) of the laser radiation in comparison to heat conduction welding. Due to multiple reflexions within the highly dynamic keyhole, the absorption mechanisms are very complex. The questions, how a laser beam interacts with the existing keyhole, and, if shadowing effects occur, are a matter of concern for several researchers. In this study, the hypothesis that the beam of a laser source can be transmitted to a significant extent through an existing keyhole and acts predominantly at the keyhole bottom was investigated. Experiments were carried out on mild steel and technical pure aluminum, using a specially designed optical system, which allows to coaxially combine two laser beams and to adjust their settings like the energy and the focal plane individually. A combination of a disk laser with a focal diameter of 390 μm and a single-mode fiber laser with a focal diameter of 30 μm was used. Weld depths and seam shapes were analyzed in cross and longitudinal sections. Based on the results, it is shown that the much smaller focal diameter of the single-mode laser beam acted at the bottom of the keyhole and caused a kind of “keyhole-in-keyhole formation” in the form of a local maximum in weld depth whose expression depended on the focal plane of the single-mode laser beam.

Keywords Laser beam welding · Keyhole behavior · Beam shaping · Multi focus · Ray tracing

1 Introduction

Laser deep penetration welding is known to produce narrow and deep weld seams with a comparatively small heat affected zone [1]. By exceeding a threshold intensity, evaporation and the formation of a vapor capillary called keyhole are caused, which is maintained by the steam pressure from the vapor being generated [2], resulting in higher absorption rates as a result of multiple reflexions of the laser beam in the keyhole [3]. The depth of the keyhole can either be

determined by optical coherence tomography (OCT) measurement or based on metallographic cross-sections, since the weld depth determined there corresponds approximately to the keyhole depth [4] and the OCT measurement [5]. Due to interaction of solid, liquid, and gaseous material, the physical phenomena occurring during the process are quite complex and, as the pressure in the keyhole oscillates at high frequencies [6], the process of laser deep penetration welding is highly dynamic. Measured frequencies reach from less than 100 Hz created by melt pool oscillations [7] to fluctuations observed at the keyhole front wall with frequencies up to 100 kHz [8]. Due to material properties such as a lower viscosity, changed keyhole behaviors including increased dynamics and instabilities such as spatter and pore formation can be observed in aluminum compared to steels [9].

The plasma, which is created by the ionized metal vapor mixed with ambient gases, plays an essential role for the energy transport from the laser beam to the workpiece [10]. It may affect the complex absorption mechanism by influencing the resulting laser beam power within the keyhole, the beam radius, and divergence depending on the laser beam properties [11]. The absorption mechanism in a

Recommended for publication by Commission IV - Power Beam Processes

✉ M. Möbus
moebus@bias.de

P. Woizeschke
peer.woizeschke@tu-dortmund.de

¹ BIAS - Bremer Institut Für Angewandte Strahltechnik GmbH, Klagenfurter Str. 5, 28359 Bremen, Germany

² TU Dortmund University, Professorship LMP+, affiliated With ISF, Baroper Straße 303, 44227 Dortmund, Germany

plasma is mainly inverse bremsstrahlung [12] and depends quadratically on the wavelength [13], resulting in 100 times higher plasma absorption rates for CO₂ laser beams with a wavelength of approximately 10 μm than for laser beams with a wavelength of approximately 1 μm, such as Nd:YAG, fiber, or disk laser sources. [14]. While the energy absorbed in the plasma inside the keyhole can be partially released back to the keyhole wall, the energy absorbed in the plasma above the keyhole is almost completely not introduced into the workpiece. In the field of laser deep penetration welding of metal sheets with high laser beam intensities, the effect of plasma shielding (decrease of the penetration depth despite increase of the laser power or line energy) has therefore also been observed above the keyhole due to a possibly too high absorption of the laser beam energy in the torch, especially in CO₂ laser beam processes [13]. When using laser sources with a wavelength of 1 μm, this phenomenon does not usually occur.

Numerical simulations, which are also increasingly used in the field of laser beam welding to gain a deeper understanding of the process, for optimization and for minimizing production problems, must take into account these highly complex and dynamic process properties. In spite of the rising computer efficiency, a complete simulation of the entire process of laser deep penetration welding is currently not fully conceivable [15]. Instead, numerical codes are constrained to simulate the process scale by scale and to concatenate results, starting with the laser–material interaction (multiple reflection) which gives the heat input to a heat transfer and fluid flow calculation [15]. In order to implement this, raytracing algorithms are a simple technique used by many researchers when it comes to analyzing the keyhole behavior [16], molten pool dynamics [17], mechanisms leading to defect occurrence [18], and absorption conditions within the keyhole [19]. In the process of raytracing, the dimensional aspects and the energy distribution of the laser beam are taken and discretized in rays with the objective to compute, one by one, the ray properties and their interaction

with the vapor/liquid interface [15]. For this, the assumption is made, that the region of gas or plasma can be treated as a void into which the laser beam can enter and pass through without being influenced until it hits the surface of the keyhole and interactions occur [17]. So far, this assumption could not be confirmed, meaning that it was not clear if a laser beam can be transmitted through an existing keyhole without getting affected by vapor, plasma, or the fluctuating keyhole itself.

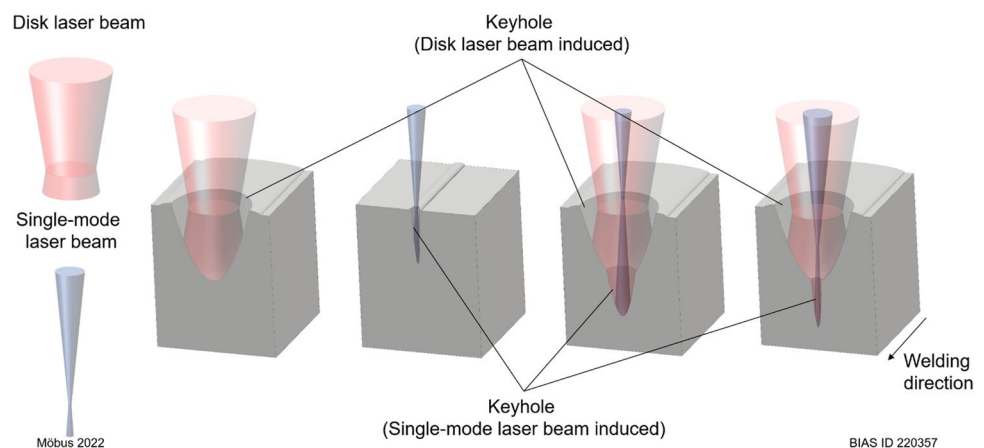
This study investigates the hypothesis that the narrower beam of an additional laser source can be transmitted to a significant extent through an existing wider keyhole generated by the initial laser beam and acts predominantly at its keyhole bottom. Therefore, a laser processing optic was used that coaxially combines two individual and freely adjustable laser beam sources. It is assumed that the highly focused second laser beam forms an additional narrower keyhole peak at the original keyhole bottom, i.e., a kind of keyhole-in-keyhole. Since the welding depth depends strongly on the focal plane of the laser, depending on the focal position of the second laser beam and thus the local beam diameter at the initial keyhole bottom, the shape of the additional keyhole peak would have to vary. Figure 1 illustrates the hypothesis as well as the derived assumptions.

2 Experimental

2.1 Setup for welding experiments

The experiments were carried out by using a custom-made laser processing optic system (Fig. 2), which is described in more detail in [20]. It coaxially combined two individual laser beams and an additional OCT measuring beam. The optics contained one dichroic mirror that reflected a wavelength of 1030 nm, distributed by the disk laser source TruDisk12002 (TRUMPF GmbH + Co. KG), and transmitted the wavelength range of 800 nm to 900 nm used by the

Fig. 1 Illustration of the hypothesis that the highly focused beam of a single-mode laser source can be transmitted through an existing keyhole, induced by a disk laser source with a wider focal diameter, and act predominantly at the keyhole bottom depending on its focal plane



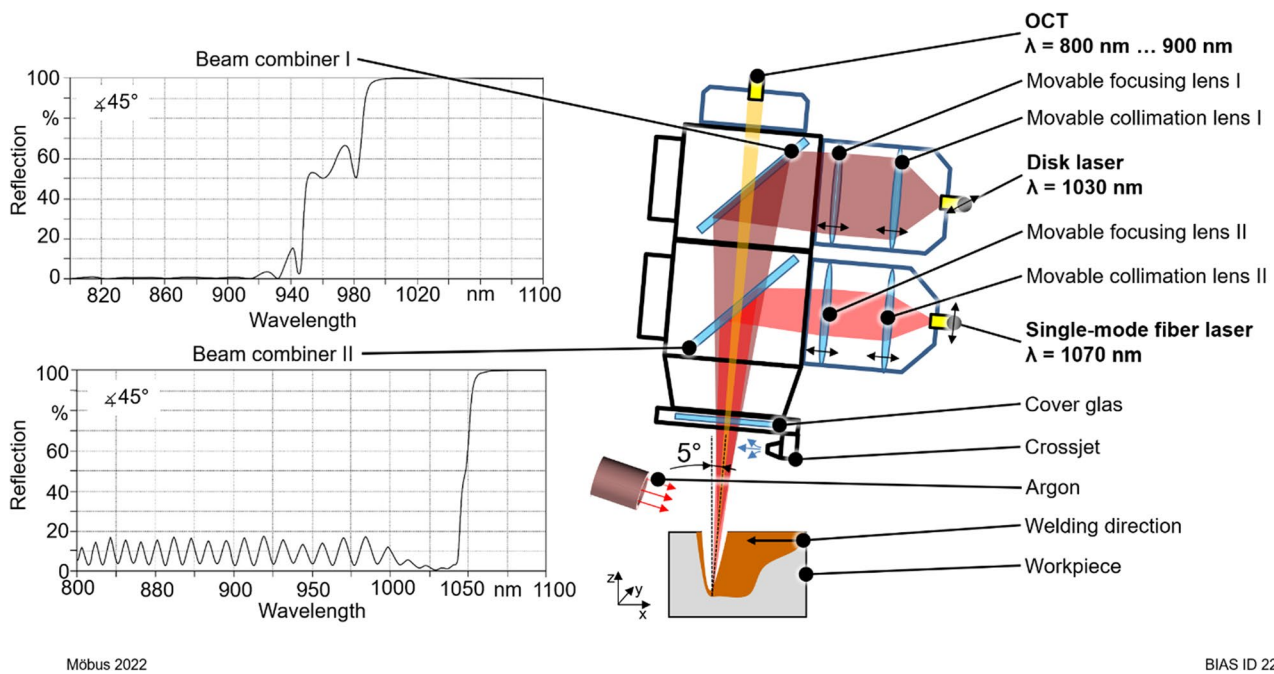


Fig. 2 Schematical laser processing and experimental setup (OCT: optical coherence tomography)

Table 1 Constant settings of the laser beams

Manufacturer	Disk laser Trumpf TruDisk12002	Single-mode fiber laser IPG-YLR-1000SM
Wavelength λ	1030 nm	1070 nm
Fiber diameter d_{Fi}	200 μm	14 μm
Focal length of the collimating lens	200 mm	200 mm
Focal length of the focusing lens	400 mm	350 mm
Measured focus diameter	390 μm	30 μm
Angle of incidence	5°	5°
M^2	25.1	1.20
Rayleigh length	4.2 mm	0.52 mm

OCT system Laser Depth Dynamics LD-600 (Laser Depth Dynamics Inc.; nowadays part of IPG Photonics Corporation). The second integrated dichroic mirror transmitted both of the aforementioned wavelength ranges and reflected a wavelength of 1070 nm, which was provided by a single-mode fiber laser source YLR-1000SM (IPG Photonics Corporation). The collimation and focusing lenses were positioned in front of the dichroic mirrors when looking in the beam direction from the source to the workpiece. This allowed to set the focal plane of each laser source individually with an accuracy of $\pm 50 \mu\text{m}$ along the beam axis by moving the positions of the lenses within the beam path. Beam parameters as the focal diameter and the Rayleigh length, as well as the power, could also be set independently of each other. The settings and properties of the two laser sources used in this study can be seen in Table 1. The

intensity profiles in the focal plane for both laser beams as well as their combination, measured by the HighPowerMSM (Primes GmbH), are given in Fig. 3.

To investigate the influences of both laser sources on different specimen materials, bead-on-plate welding experiments were carried out using mild steel S235JRC and technical pure aluminum EN AW-1050A H111 (Al99.5), whose compositions are given in Table 2.

The experimental program is shown in Table 3 (steel) and Table 4 (aluminum). Apart from the material and the used laser powers, both material-specific plans are comparable, including one sample welded with 3000 W (steel) resp. 3700 W (aluminum) laser power from TruDisk12002, which is the maximum power (named 100%) used in each experimental plan. The maximum power of 3700 W for aluminum was chosen to match the same weld depth which is caused by

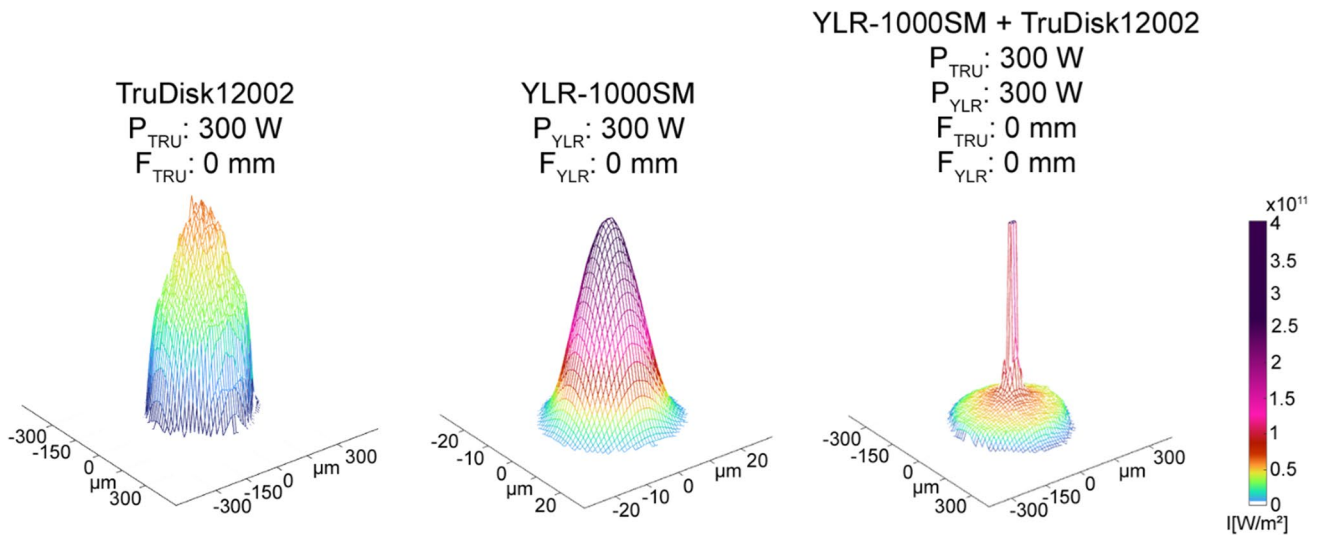


Fig. 3 Intensity profiles of the used laser beams and their combination measured in the focal plane (P: laser power used for measurement, F: measured focal position, I: intensity)

Table 2 Chemical composition of S235JRC according to [21] (left) and chemical composition of EN AW-1050A H111 (Al99.5) according to [22] (right)

Chemical composition of S235JRC (wt.%)						
Fe	Mn	Cu	Si	Cr	Ni	C
Bal	0.520	0.230	0.200	0.160	0.130	0.080

Chemical composition of EN AW-1050A H111 (wt.%)						
Al	Fe	Si	Zn	Ti	Mg	Cu
99.663	0.234	0.054	0.005	0.004	0.002	0.002

Table 3 Experimental plan S235JRC

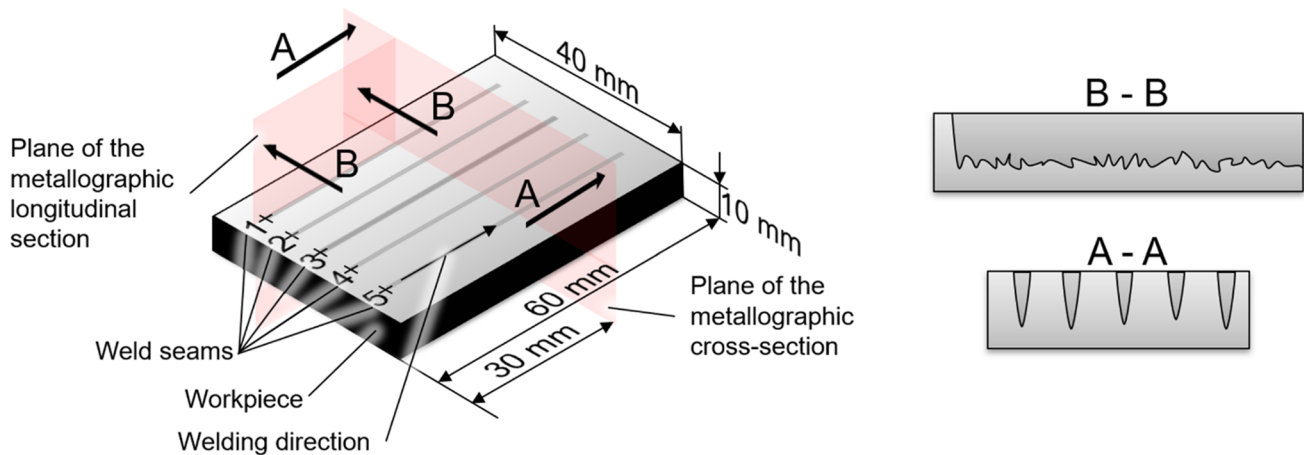
Material	Total power (W)	Power TruDisk12002 (W)	Power YLR-1000SM (W)	Focal plane TruDisk12002 (mm)	Focal plane YLR-1000SM (mm)
S235JRC	3000	3000	-	0	-
S235JRC	2400	2400	-	0	-
S235JRC	600	-	600	-	0
S235JRC	3000	2400	600	0	0
S235JRC	3000	2400	600	0	-2
S235JRC	3000	2400	600	0	-4
S235JRC	3000	2400	600	0	-6
S235JRC	3000	2400	600	0	-8

3000 W in steel. One sample was welded only with the TruDisk12002 laser beam at approximately 80% power (2400 W steel and 3100 W aluminum, respectively) and one sample only with the YLR-1000SM laser beam at approximately 20% power (600 W steel and 600 W aluminum, respectively). All other samples were welded with a combination of both laser beams, with a constant power distribution of about 80% TruDisk12002 and 20% YLR-1000SM, varying only the focal plane of the YLR-1000SM (F_{YLR}) from “0” to “-8 mm.”

Figure 2 also shows the experimental welding setup. The specimen was placed on a moving table, which provided a constant welding speed of 2 m/min. The irradiation angle of the processing setup was tilted by 5° to the vertical orientation against the welding direction, resulting in forehand welding. Argon was used as shielding gas with a flow rate of 7 l/min and a nozzle diameter of 8 mm. The size of the specimen and the seam lengths of 50 mm are given in Fig. 4. On a single specimen, each

Table 4 Experimental plan EN AW-1050 H111

Material	Total power (W)	Power TruDisk12002 (W)	Power YLR-1000SM (W)	Focal plane TruDisk12002 (mm)	Focal plane YLR-1000SM (mm)
EN AW-1050A H111	3700	3700	-	0	-
EN AW-1050A H111	3100	3100	-	0	-
EN AW-1050A H111	600	-	600	-	0
EN AW-1050A H111	3700	3100	600	0	0
EN AW-1050A H111	3700	3100	600	0	-2
EN AW-1050A H111	3700	3100	600	0	-4
EN AW-1050A H111	3700	3100	600	0	-6
EN AW-1050A H111	3700	3100	600	0	-8



Möbus 2022

BIAS ID 220360

Fig. 4 Dimensions and design of the specimen (specimen was changed after every single welding process to let the specimen temperature decrease to room temperature before the next weldment)




parameter listed in Tables 3 and 4 was repeated five times. However, the specimen was changed after every single welding process to let the specimen temperature decrease to room temperature before the next weldment. The execution of the experimental plans was random. Cross-sections were taken from the center of the seam of each sample (cf. Fig. 4 A-A) and longitudinal-sections of the first seam from selected samples (cf. Fig. 4 B-B). Steel samples were etched with 1% nitric acid, and aluminum samples with 20% sodium hydroxide solution. Due to the difficulty of catching the very narrow weld peak in the center in the longitudinal sections, especially in the case of welds produced by the single-mode laser, the weld depth was determined based on the average of the 5 cross-sections. A MATLAB (MATrix LABORatory by MathWorks)-based algorithm, which analyzed pictures of the etched metallographic cross-sections, was applied to measure the size of the cross-section areas of the seams based on contrast differences and output the average seam area from the 5 cross-sections.



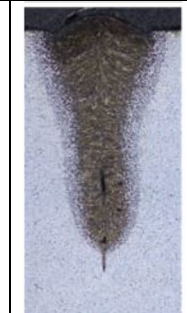
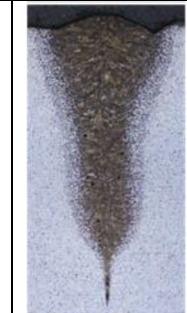

3 Results

3.1 Steel

Table 5 shows characteristic metallographic cross-sections of the welded steel samples. From 3.0 kW TruDisk12002 to 2.4 kW TruDisk12002, the weld depth decreases, whereby the rest of the seam shape remains comparable. For 0.6 kW YLR-1000SM, the weld depth resembles the weld depth of 2.4 kW TruDisk12002, but the seam shape is significantly narrower resulting in a sharp peak at the bottom of the seam. In comparison, the seam shapes of the samples with combined laser beams (2.4 kW TruDisk12002 and 0.6 kW YLR-1000SM) show no clear addition of the individual seam cross-sections for steel, as the seam welded by the single-mode laser beam only is much more pronounced. Nevertheless, it can be seen that, while at $F_{YLR} = -8$ mm, no significant difference in seam form to 3.0 kW TruDisk12002 without YLR-1000SM superposition is noticeable, with increasing focal plane and local

Table 5 Exemplary metallographic cross-sections of welded steel samples

Power TruDisk12002	3.0 kW	2.4 kW	-
PowerYLR-1000SM	-	-	0.6 kW
Focal Plane TruDisk12002	0 mm	0 mm	
Focal Plane YLR-1000SM	-	-	0 mm
Metallographic cross-section			

Power TruDisk12002	2.4 kW	2.4 kW	2.4 kW	2.4 kW	2.4 kW
Power YLR-1000SM	0.6 kW	0.6 kW	0.6 kW	0.6 kW	0.6 kW
Focal Plane TruDisk12002	0 mm	0 mm	0 mm	0 mm	0 mm
Focal Plane YLR-1000SM	-8 mm	-6 mm	-4 mm	-2 mm	0 mm
Metallographic cross-section					

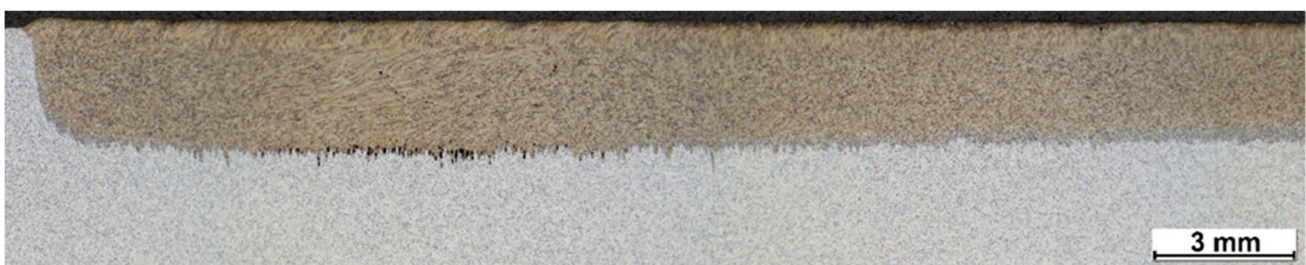
Möbus 2022

BIAS ID 220361

intensity at the bottom by the single-mode laser beam; the weld depth increases; and a local peak at the bottom of the seam is formed which becomes increasingly pronounced as the focal plane of the single-mode laser beam approaches the disk laser beam induced keyhole bottom and then also decreases as the focal plane is further increased to

$F_{YLR} = 0$ mm. With all combinations, we also see that the size of the upper "base seam" is larger than the seam welded with only 2.4 kW of the disk laser source and that it also increases from $F_{YLR} = -8$ mm to $F_{YLR} = -2$ mm.

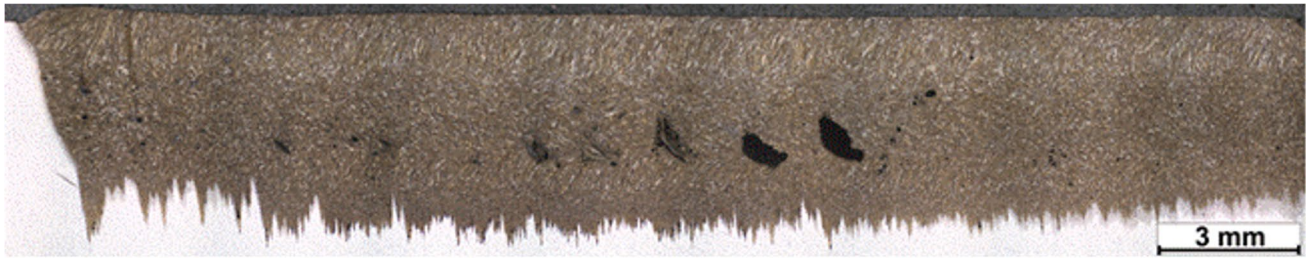
In Fig. 5, the longitudinal section and the weld depth in seam direction for 0.6 kW YLR-1000SM at $F_{YLR} = 0$ mm are shown.



Möbus 2022

BIAS ID 220362

Fig. 5 Exemplary metallographic longitudinal-section of a steel sample welded with 0.6 kW YLR-1000SM at the focal plane $F_{YLR} = 0$ mm



Möbus 2022

BIAS ID 220362

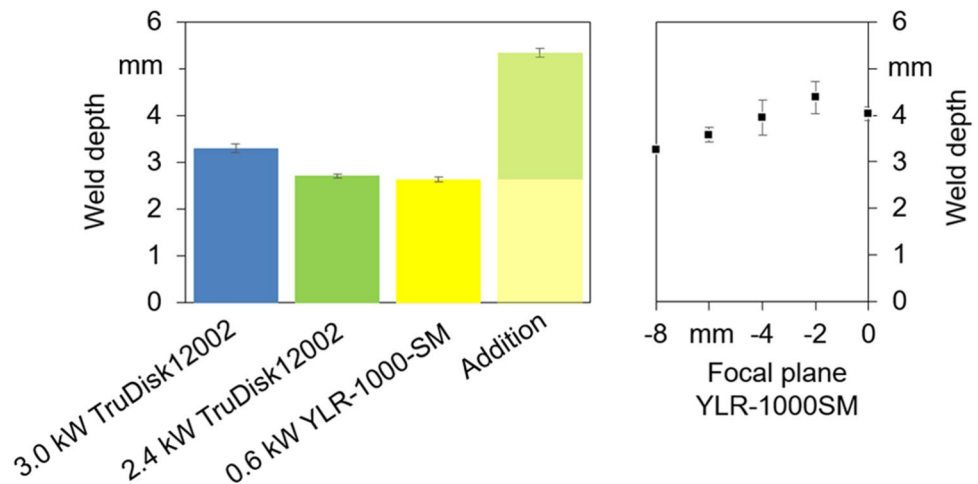
Fig. 6 Exemplary metallographic longitudinal-section of a steel sample welded with the combination of 2.4 kW TruDisk12002 and 0.6 kW YLR-1000SM for the focal plane $F_{YLR} = -2$ mm

Especially in a range of about 5 to 10 mm after the start of the weld, relatively uniform fluctuations in the weld depth can be observed so that it can be assumed that the keyhole depth fluctuates slightly. This is only clearly visible in an area of about 5 mm, which is due to the fact that the seam was not hit exactly in the center due to the very narrow width, and therefore, only this area characterizes the seam center. The longitudinal section presented in Fig. 6 shows the weld depth in seam direction for the combination of 2.4 kW TruDisk12002 and 0.6 kW YLR-1000SM at $F_{YLR} = -2$ mm. The slightly fluctuating weld depth, which can be seen in the cross-section in Table 5, is also visible but significantly stronger, while its average, however, corresponds to the average of the 5 cross-sections.

The results of the weld depths for the different used laser beams, beam combinations, laser powers, and focal planes are presented in Fig. 7. Furthermore, the idealized theoretical sum of the weld depths of the single-beam variants with 2.4 kW TruDisk12002 and 0.6 kW YLR-1000SM is added. It can be seen that the average weld depth decreased slightly from 3.30 mm at 3 kW TruDisk12002 (blue bar) to 2.71 mm at 2.4 kW TruDisk12002 (green bar) and further to 2.63 mm

at 0.6 kW YLR-1000SM (yellow bar). This means that the weld depth of the 2.4 kW disk laser-induced seam (2.71 mm) lies between the selected focal planes of the YLR-1000SM $F_{YLR} = -4$ mm and $F_{YLR} = -2$ mm. The theoretical sum of the two last mentioned separate processes is 5.34 mm (green/yellow bar), whose power add up to a theoretical overall power of 3.0 kW, and is significantly higher than the weld depth of the comparable process with 3 kW of the TruDisk12002 alone. The weld depths according to the real experimental combinations of both laser beams as function of the focal plane position of the YLR-1000SM beam, with a constant focal plane of the TruDisk12002 beam at 0 mm, are also displayed on the right in Fig. 7. It can be seen that the measurement data clearly support the observations from the cross-sections that there is no clear addition of the welding depths of the individual tests in the combined test since all weld depths from $F_{YLR} = -8$ mm to $F_{YLR} = 0$ mm are below the value of the theoretical sum, but equal or over the weld depth of the 3.0 kW of the TruDisk12002 alone, rising from $F_{YLR} = -8$ mm (3.26 mm) to its maximum at -2 mm (4.38 mm).

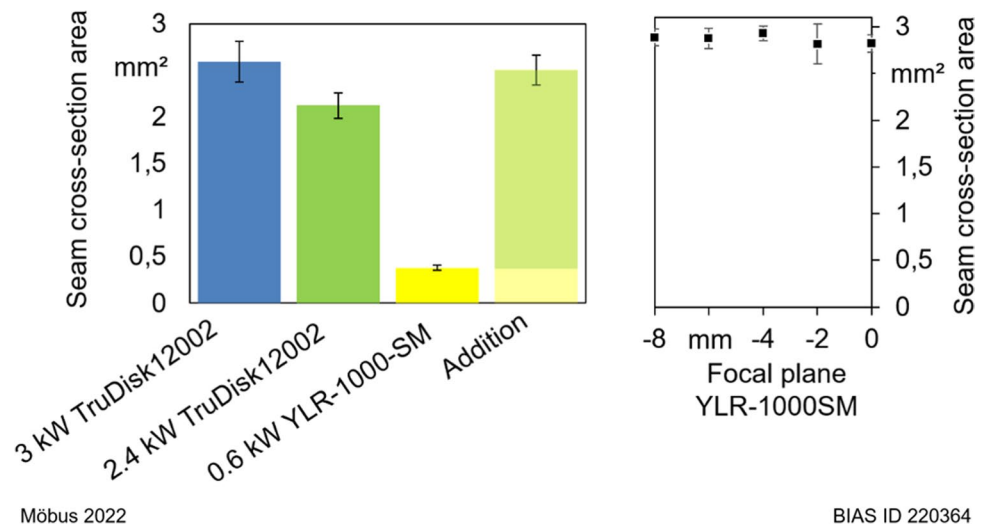
Fig. 7 Left: Influence of the laser beam power and the laser source on the weld depth in S235JRC (all focal planes at 0 mm) and theoretical sum of the weld depth of 2.4 kW TruDisk12002 and 0.6 kW YLR-1000SM. Right: Influence of the focal plane of the coaxially superimposed single-mode laser beam (0.6 kW) in disk laser deep penetration welding (2.4 kW, focal plane 0 mm) on the weld depth in S235JRC



Möbus 2022

BIAS ID 220363

Fig. 8 Left: Influence of the laser beam power and the laser source on the seam cross-section area in S235JRC (all focal planes at 0 mm) and theoretical sum of the seam cross-section area of 2.4 kW TruDisk12002 and 0.6 kW YLR-1000SM. Right: Influence of the focal plane of the coaxially superimposed single-mode laser beam (0.6 kW) in disk laser deep penetration welding (2.4 kW, focal plane 0 mm) on the seam cross-section area in S235JRC



The resulting average cross-section areas of the seams are presented in Fig. 8 with equal x -axis and colors than already used in Fig. 7. The seam cross-section area decreases slightly from 2.59 mm² at 3.0 kW TruDisk12002 (blue bar) to 2.12 mm² at 2.4 kW TruDisk12002 (green bar), whereby it drops sharply to 0.38 mm² at 0.6 kW YLR-1000SM (green bar), resulting in a theoretically added seam cross-section area (green/yellow bar) of 2.50 mm², which is just below the value of the 3.0 kW TruDisk12002. The seam cross-section areas of the experimental combinations are above the values of the 3.0 kW TruDisk12002 and the theoretical sum and differ only slightly between 2.82 mm² ($F_{\text{YLR}} = -2$ mm) and 2.93 mm² ($F_{\text{YLR}} = -4$ mm).

3.2 Aluminum




Table 6 shows characteristic metallographic cross-sections of the welded aluminum samples. From 3.7 kW TruDisk12002 to 3.1 kW TruDisk12002, the weld depth decreases, whereby the actual shape of the seam remains comparable. The seam shape of the sample welded with 0.6 kW YLR-1000SM is, in contrast, significantly narrower with an even more reduced weld depth. As seen for steel, the seam shapes of the samples with combined laser sources (3.1 kW TruDisk12002 and 0.6 kW YLR-1000SM) differ with different focal planes of the YLR-1000SM but show no clear addition of the individual seam cross-sections forms. At $F_{\text{YLR}} = -8$ mm, no big difference to 3.7 kW TruDisk12002 can be seen in weld depth or seam shape but with increasing focal plane and local intensity at the bottom by the single-mode laser beam, the weld depth increases, and a local peak at the bottom of the seam is formed which also becomes increasingly pronounced as the focal plane of the single-mode laser beam approaches the disk laser beam-induced keyhole






bottom and then also decreases as the focal plane is further increased to $F_{\text{YLR}} = 0$ mm. As with steel, it can be seen that the size of the upper “base seam” cross-section shape also increases for the combination compared to 3.1 kW disk laser beam only.

The longitudinal section, presented in Fig. 9, shows the weld depth in seam direction for the combination of 3.1 kW TruDisk12002 and 0.6 kW YLR-1000SM at $F_{\text{YLR}} = -2$ mm. The fluctuating weld depth which can be seen in the cross-section in Table 6, and which average corresponds to the average weld depth of the 5 cross-sections, is also visible in the longitudinal section. In comparison to the longitudinal section of the steel sample, these maxima occur less frequently and have a wider shape. Pores within the seam can be detected.

The results of the weld depths in aluminum over the different used laser sources, their combination, and their power and focal plane are presented in Fig. 10. The theoretical sum of the weld depths of the processes with 3.1 kW TruDisk12002 and 0.6 kW YLR-1000SM is also shown. It can be seen that the average weld depth constantly decreases from 3.19 mm at 3.7 kW TruDisk12002 (blue bar) to 2.47 mm at 3.1 kW TruDisk12002 (green bar) to 1.37 mm at 0.6 kW YLR-1000SM (yellow bar). As for steel, this means that the weld depth of the 3.1 kW disk laser-induced seam (2.47 mm) lies between the selected focal planes $F_{\text{YLR}} = -4$ mm and $F_{\text{YLR}} = -2$ mm. The theoretical sum of the weld depth of 3.1 kW TruDisk12002 and 0.6 kW YLR-1000SM is with 3.84 mm (green/yellow bar) only slightly above the value of 3.7 kW TruDisk12002. The weld depth of the real experimental combination of both laser sources over the focal plane of the YLR-1000SM with a constant focal plane of the TruDisk12002 at 0 mm is displayed on the right in Fig. 10. As seen in the cross-section results, the

Table 6 Exemplary metallographic cross-sections of welded aluminum samples

Power TruDisk12002	3.7 kW	3.1 kW	-
Power YLR-1000SM	-	-	0.6 kW
Focal Plane TruDisk12002	0 mm	0 mm	-
Focal Plane YLR-1000SM	-	-	0 mm
Metallographic cross-section			

Power TruDisk12002	3.1 kW	3.1 kW	3.1 kW	3.1 kW	3.1 kW
Power YLR-1000SM	0.6 kW	0.6 kW	0.6 kW	0.6 kW	0.6 kW
Focal Plane TruDisk12002	0 mm	0 mm	0 mm	0 mm	0 mm
Focal Plane YLR-1000SM	-8 mm	-6 mm	-4 mm	-2 mm	0 mm
Metallographic cross-section					

Möbus 2022

BIAS ID 220365



Möbus 2022

BIAS ID 220365

Fig. 9 Exemplary metallographic longitudinal-section of an aluminum sample welded with the combination of 3.1 kW TruDisk12002 and 0.6 kW YLR-1000SM for the focal plane $F_{YLR} = -2$ mm

weld depth of 3.01 mm for the combination of both laser sources at $F_{YLR} = -8$ mm resembles the weld depth of 3.7 kW TruDisk12002 alone, rising to a maximum weld

depth of 4.02 mm at $F_{YLR} = -2$ mm which is higher than the weld depth of the theoretical sum of 3.1 kW TruDisk12002 and 0.6 kW YLR-1000SM.

Fig. 10 Left: Influence of the laser beam power and the laser source on the weld depth in EN AW-1050 H111 (all focal planes at 0 mm) and theoretical sum of the weld depth of 3.1 kW TruDisk12002 and 0.6 kW YLR-1000SM. Right: Influence of the focal plane of the coaxially superimposed single-mode laser beam (0.6 kW) in disk laser deep penetration welding (3.1 kW, focal plane 0 mm) on the weld depth in EN AW-1050 H111

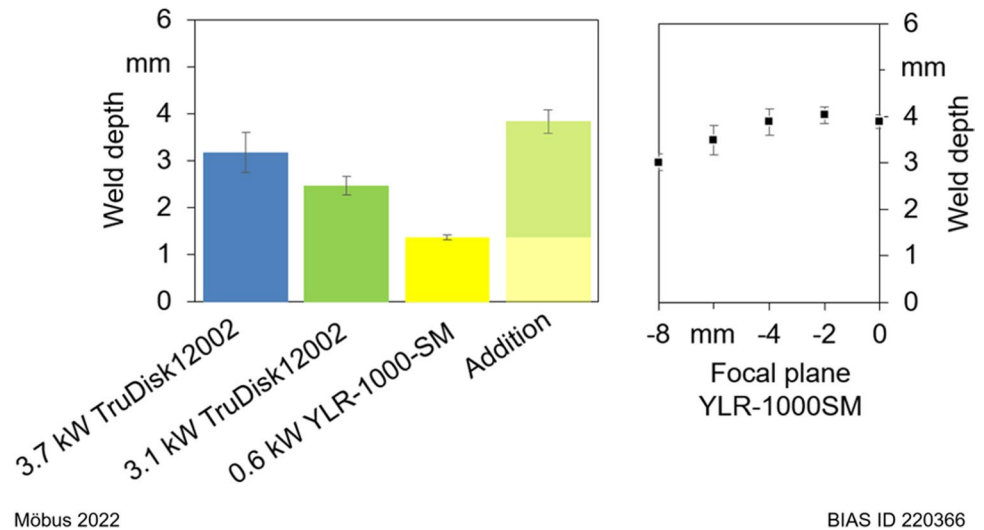
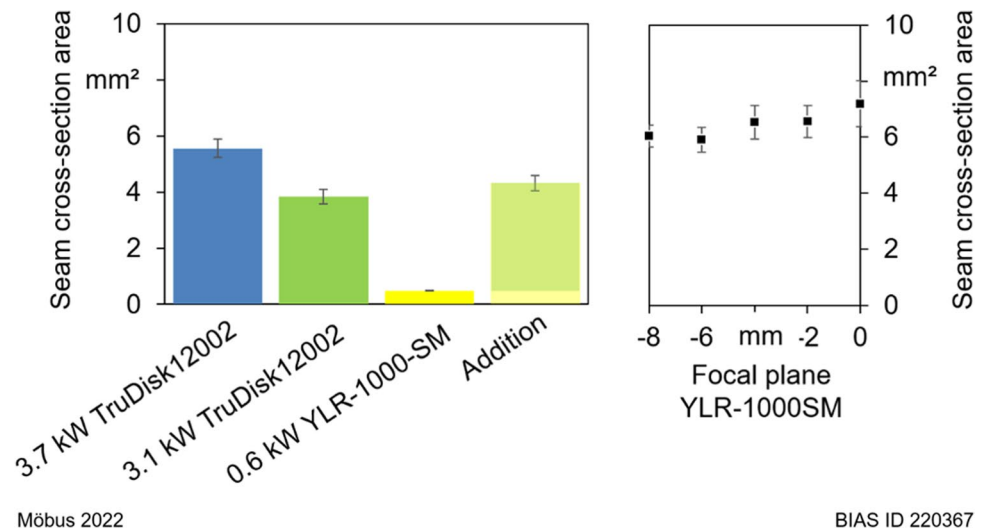


Fig. 11 Left: Influence of the laser beam power and the laser source on the seam cross-section area in in EN AW-1050 H111 (all focal planes at 0 mm) and theoretical sum of the seam cross-section area of 3.1 kW TruDisk12002 and 0.6 kW YLR-1000SM. Right: Influence of the focal plane of the coaxially superimposed single-mode laser beam (0.6 kW) in disk laser deep penetration welding (3.1 kW, focal plane 0 mm) on the seam cross-section area in EN AW-1050 H111



The resulting average cross-section areas of the aluminum seams are presented in Fig. 11. The seam cross-section area decreases slightly from 5.56 mm² at 3.7 kW TruDisk12002 (blue bar) to 3.84 mm² at 3.1 kW TruDisk12002 (green bar), whereby it drops significantly to 0.48 mm² at 0.6 kW YLR-1000SM (yellow bar), resulting in a theoretically summed seam cross-section area of 4.32 mm² (green/yellow bar), which is below the value of 3.7 kW TruDisk12002. As already seen with the steel samples, all seam cross-section areas of the experimental combinations are above the values of the 3.7 kW TruDisk12002 and the theoretical sum and differ between 5.90 mm² ($F_{YLR} = -6$ mm) and 7.19 mm² ($F_{YLR} = 0$ mm). Compared to the average cross-section areas of the steel seams, the cross-section areas of the aluminum seams show the same peculiarities, whereas all their values except for the 0.6 kW YLR-1000SM only are approximate twice as high as the values of steel.

4 Discussion

In the following, the hypothesis that the narrower beam of an additional laser source can be transmitted to a significant extent through an existing wider keyhole generated by the initial laser beam, acts predominantly at the bottom of the keyhole by forming an additional narrower keyhole peak, i.e., a kind of keyhole-in-keyhole, is evaluated.

For both materials, some addition effect of the welding depths can be confirmed, since nearly all weld depth of the combined process exceed the values for the only disk laser powered processes and the measured maximum weld depth, which was observed for both materials at $F_{YLR} = -2$ mm, is even slightly above the idealized value of the sum of the individual processes for aluminum, and is only slightly below the idealized value of the sum of the individual

processes for steel. However, a clear addition of the two seam shapes could not be observed for both materials, since the seam that was welded with 0.6 kW single-mode laser is clearly more pronounced than the peaks in the weld depth that can be seen in the cross-sections of the combinations. The cross-section of the seam made from the steel sample (Table 5; $F_{\text{YLR}} = -2$ mm), which allows conclusions to be drawn about the keyhole depth [4], can be divided into two parts. The upper part of the seam and thus of the former keyhole has a shape comparable to the shape of 3 kW disk laser beam only, meaning that it was mainly induced by the disk laser beam. Since the size of the upper, mainly disk laser-induced cross-section shape, increases for the combination compared to 2.4 kW for steel, respectively, 3.1 kW disk laser beam for aluminum, it can be concluded that there is also an energy input from the single-mode laser beam into the mainly disk laser beam-induced keyhole for both materials. The lower, pointed part of the seam was mainly induced by the single-mode laser beam as the shape is comparable to the bottom of the shape of the seam welded with 0.6 kW single-mode laser beam only. The described division of the seam into a mainly disk laser beam induced and a mainly single-mode laser beam-induced part means that the single-mode laser beam was to a significant extent transmitted through the disk laser induced keyhole, created an additional narrower keyhole peak at its bottom, and thus caused a kind “keyhole-in-keyhole formation,” regardless of the material, which supports the hypothesis.

When looking at the longitudinal sections (Figs. 6 and 9), however, it becomes clear that the additional keyhole tip leads to an unstable overall keyhole shape. The keyhole strives to adopt a more stable shape, which results in periodic inconstant welding behavior in the longitudinal direction of the seam. As was mentioned above, especially in laser deep welding of aluminum, the keyhole is also inherently unstable, which can cause the keyhole to collapse [9] or high dynamic keyhole shape changes. If this happens, the single-mode laser beam temporary can no longer hit the bottom of the disk laser induced keyhole and thus cannot cause a local deepening of the weld depth. For this reason, the effect occurs much more frequently in steel as the keyhole is much more stable. Looking at the longitudinal section of the sample welded with 0.6 kW YLR-1000SM at $F_{\text{YLR}} = 0$ mm (Fig. 5), it becomes clear that the deep fluctuations are caused by the combination of both laser beams and the addition of their intensities in the seam center, since they cannot be seen to a similar depth here.

Based on the cross-sections, it could also be shown that the weld depth and the expression of the peaks have their measured maximum at $F_{\text{YLR}} = -2$ mm for both materials. Making the assumption that the keyhole depth corresponds approximately to the weld depth measured in cross-sections [4], the depth of the disk laser beam-induced

keyhole was 2.71 mm in steel, as measured for 2.4 kW disk laser beam power only (cf. Fig. 7), and 2.47 mm in aluminum, as measured for 3.1 kW disk laser beam power only (Fig. 10). Assuming further that the single-mode laser beam set to $F_{\text{YLR}} = -2$ mm transmitted through the disk laser beam-induced keyhole, it was therefore focused closest to its bottom. Changing the value to $F_{\text{YLR}} = -4$ mm or $F_{\text{YLR}} = -0$ mm resulted in defocusing relative to the disk laser beam-induced keyhole bottom and a lower intensity, which was followed by a wider diameter and a lower depth of the single-mode laser beam additionally induced keyhole tip. This shows the clear correlation between the focal plane and the weld penetration depth and indicates that a maximum weld depth would be expected if the focal plane of the YLR-1000SM had been exactly set on the former disk laser beam-induced keyhole bottom, supporting the confirmation of the hypothesis. Furthermore, it could be a possible explanation why the idealized value of the theoretical sum of the weld depth could not be reached in case of steel but aluminum. Since the distance between the focal plane and the average depth of the disk laser beam-induced keyhole bottom (0.71 mm for steel, 0.47 mm for aluminum) exceeds the Rayleigh length of 0.51 mm of the single-mode laser beam for steel, but not for aluminum, the intensity of the laser beam at the keyhole bottom was lower for steel, resulting in a lower weld penetration depth. This also indicates that the results of the weld depth of steel and aluminum compared to the idealized theoretical sum can hardly be compared, since the same distance between the focal plane of the single-mode laser beam and the disk laser beam-induced keyhole bottom was not achieved and fluctuations in weld depth could be seen. From the increased cross-section areas of the combinations compared to the theoretical sums, it can be concluded that the total coupling of the laser radiation increases for steel and for aluminum which may also explain why the weld depth in aluminum exceeds the theoretical sum of the individual processes.

5 Conclusions

In this study, a specially designed optical system, which allows to coaxially combine two laser beams and adjust their settings like the power and the focal plane individually has been used to investigate the hypothesis that the narrower beam of an additional laser source can be transmitted to a significant extent through an existing wider keyhole generated by the initial laser beam, acts predominantly at the bottom of the keyhole by forming an additional narrower keyhole peak, i.e., a kind of keyhole-in-keyhole. For this purpose, combinations of a disk laser beam and a single-mode fiber laser beam with different focal planes were investigated. Effects of the single-mode fiber laser beam at

the bottom of the seam as a function of its focal position could be visualized in the form of a peak in the weld depth due to a kind of “keyhole-in-keyhole formation.” Two conclusions can be drawn:

- (1) The hypothesis that the narrower beam of an additional laser source can be transmitted to a significant extent through an existing wider keyhole generated by the initial laser beam, acts predominantly at the bottom of the keyhole by forming an additional narrower keyhole peak, i.e., a kind of keyhole-in-keyhole, could be confirmed, whereby the effect has so far always fluctuated and not been stable.
- (2) With regard to the expression of the keyhole peak, a clear influence of the focal plane of the additional laser source could be identified.

Funding Open Access funding enabled and organized by Projekt DEAL. The authors received funding from the German Research Foundation (Deutsche Forschungsgemeinschaft DFG, project number 423364400).

Declarations

Conflict of interest The authors declare no competing interests.

Open Access This article is licensed under a Creative Commons Attribution 4.0 International License, which permits use, sharing, adaptation, distribution and reproduction in any medium or format, as long as you give appropriate credit to the original author(s) and the source, provide a link to the Creative Commons licence, and indicate if changes were made. The images or other third party material in this article are included in the article's Creative Commons licence, unless indicated otherwise in a credit line to the material. If material is not included in the article's Creative Commons licence and your intended use is not permitted by statutory regulation or exceeds the permitted use, you will need to obtain permission directly from the copyright holder. To view a copy of this licence, visit <http://creativecommons.org/licenses/by/4.0/>.

References

1. Bley H, Weyand L, Luft A (2007) An alternative approach for the cost-efficient laser welding of zinc-coated sheet metal. *CIRP Ann* 56(1):17–20
2. Steen W, Mazumder J, Mazumder J (2010) *Laser material processing*. Springer, London
3. Steen WM (1991) *Laser material processing*, 1st edn. Springer, London
4. Mittelstädt C, Mattulat T, Seefeld T, Kogel-Hollacher M (2019) Novel approach for weld depth determination using optical coherence tomography measurement in laser deep penetration welding of aluminum and steel. *J Laser Appl* 31(2):22007
5. Pordzik R, Mattulat T, Woizeschke P (2022) Effects of reduced ambient pressure on the OCT-based weld depth measurement signal in laser welding of aluminum and steel. *Procedia CIRP* 111(4):541–546
6. Volpp J, Freimann D (2013) Indirect measurement of keyhole pressure oscillations during laser deep penetration welding. In: *Proc. of the 32nd Int. Congress on Applications of Lasers and Electro-Optics*, paper 1301, 334–340
7. Geiger M, Kägeler C, Schmidt M (2008) High-power laser welding of contaminated steel sheets. *Product Eng* 2(3):235–240
8. Kaplan AFH, Matti RS (2015) Absorption peaks depending on topology of the keyhole front and wavelength. *J Laser Appl* 27(S2):S29012
9. Dausinger F, Faisst F, Hack R, Rapp J, Hügel H, Beck M (1995) *Welding of aluminum: challenge and chance for laser technology. ICALEO® '95: Proceedings of the Laser Materials Processing Conference; November 13–16, 1995; San Diego, California, USA; In: International Congress on Applications of Lasers & Electro-Optics; Laser Institute of America 1059-1067*
10. Rai R, Elmer JW, Palmer TA, DeRoy T (2007) Heat transfer and fluid flow during keyhole mode laser welding of tantalum, Ti–6Al–4V, 304L stainless steel and vanadium. *Metall Mater Trans A* 40(18):5753–5766
11. Nonhof CJ (1988) material processing with Nd-Lasers. In: *Electrochemical, Ayz, Scotland*
12. Coviello D, D'Angola A, Sorgente D (2022) Numerical study on the influence of the plasma properties on the keyhole geometry in laser beam welding. *Front Phys* 9:2165
13. Beyer E, Diltthey U, Imhoff R, Maier C, Neuenhahn J, Behler K (1994) New aspects in laser welding with an increased efficiency. *ICALEO® '94: Proceedings of the Laser Materials Processing Conference; October 17–20, 1994; Orlando, Florida, USA; In: International Congress on Applications of Lasers & Electro-Optics; Laser Institute of America, p 183-192*
14. Greses J, Hilton PA, Barlow CY, Steen WM (2003) Laser-vapour interaction in high-power cw Nd:YAG laser welding. *ICALEO® 2003: 22nd International Congress on Laser Materials Processing and Laser Microfabrication; October 13–16, 2003; Jacksonville, Florida, USA; In: International Congress on Applications of Lasers & Electro-Optics; Laser Institute of America 1606*
15. Dal M, Fabbro R (2016) An overview of the state of art in laser welding simulation. *Opt Laser Technol* 78(1):2–14
16. Lee JY, Ko SH, Farson DF, Yoo CD (2002) Mechanism of keyhole formation and stability in stationary laser welding. *J Phys D Appl Phys* 35(13):1570–1576
17. Cho W-I, Na S-J, Thomy C, Vollertsen F (2012) Numerical simulation of molten pool dynamics in high power disk laser welding. *J Mater Process Technol* 212(1):262–275
18. Medale M, Xhaard C, Fabbro R (2007) A thermo-hydraulic numerical model to study spot laser welding. *C R Mécanique* 335(5–6):280–286
19. Cho J-H, Na S-J (2006) Implementation of real-time multiple reflection and Fresnel absorption of laser beam in keyhole. *J Laser Appl* 39(24):5372–5378
20. Möbus M, Woizeschke P (2022) Laser beam welding setup for the coaxial combination of two laser beams to vary the intensity distribution. *Weld World* 66(3):471–480
21. Andernach & Bleck GmbH & Co.KG (2020) *Abnahmeprüfzeugnis EN10204 - 3.1 - S235JRC*
22. ALCOBRA GmbH (2020) *Certificate according to EN 10204 - Aluminium products EN AW-1050A H111*

Publisher's Note Springer Nature remains neutral with regard to jurisdictional claims in published maps and institutional affiliations.